Materials Transactions, Vol. 66, No. 1 (2025) pp. 107 to 112

Measurement of Laser Absorptivity of Inconel Powders with Additive Manufacturing Machine

Hiroshi Honda* and Makoto Watanabe

Research Center for Structural Materials, National Institute for Materials Science, Tsukuba 305-0047, Japan

The nickel-based superalloy Inconel is considered suitable for near-net-shape manufacturing using additive techniques, primarily due to its machining difficulties. In laser metal-based powder-bed fusion additive manufacturing, the laser absorptivity of metal powder is one of the parameters that must be known in order to elucidate, optimize, and numerically simulate manufacturing. Therefore, we tried to measure the laser absorptivities of Inconel 718 and Inconel 738LC powders using a commercially available additive manufacturing machine.
[doi:10.2320/matertrans.MT-M2024124]

(Received August 27, 2024; Accepted October 17, 2024; Published December 25, 2024)

Keywords: *additive manufacturing, powder-bed fusion, laser absorptivity, Inconel 718 powder, Inconel 738LC powder, Ti-6Al-4V powder*

1. Introduction

The nickel-based superalloy Inconel is used in the aerospace and plant industries because of its high strength, high corrosion resistance, and high oxidation resistance at high temperature. However, it is known to be difficult to cut. Therefore, it is expected to be manufactured in near-net shape by additive manufacturing.

Laser powder-bed fusion is one of the additive manufacturing methods for metals. In this technique, laser energy absorption is a crucial initial step in the manufacturing process, with absorptivity being a key parameter for elucidating or optimizing processes. For numerical simulation of the manufacturing process, laser absorptivity is indispensable. Understanding the temperature-dependent nature of laser absorptivity is also essential for a detailed comprehension of the phenomena occurring in the manufacturing process.

One method of measuring the light absorptivity of powders is to utilize an integrating sphere. Brandau *et al.* [1] measured the absorptivity of various metal powders across a wide range of light wavelengths by using a spectrometer with an integrating sphere.

Calorimetric methods have also been used to measure the laser absorptivity of materials. Haag *et al.* [2] measured the absorptivity of aluminum, copper, iron, and titanium aluminide powders for a CO_2 laser in different atmospheres using specialized equipment. Wieting *et al.* [3] measured the laser absorptivity of stainless steel sheets in a vacuum furnace for a CO_2 laser. The temperature dependence of laser absorptivity has also been investigated by varying the furnace temperature. Rubenchik *et al.* [4, 5] assembled a measurement system with a laser diode to assess the temperature-dependent laser absorptivity without a furnace setup. The laser absorptivities of both plates and powder forms for various materials were measured [4–6]. Trapp *et al.* [7] measured the overall laser absorptivity, encompassing all phenomena that occur during the manufacturing process. The total laser absorptivities during the manufacturing processes for various laser irradiation conditions, such as laser power and scanning speed, were reported [7, 8].

Among nickel-based superalloy Inconel powders, however, there are few reports on laser absorptivity measurements specifically for Inconel 625 [6]. Further, material surface conditions change depending on the production method and the storage conditions, and surface conditions are thought to influence laser absorptivity. Therefore, measuring the laser absorptivity of powders used the powder-bed fusion additive manufacturing is considered important. The laser and the manufacturing environment, which affect laser absorptivity, vary based on the additive manufacturing machine and the manufacturing process. Therefore, it is necessary to know the laser absorptivity in each manufacturing situation in order to understand the additive manufacturing process and realize the desired product.

In a previous study [9], we proposed a simple method of measuring laser absorptivity under the same circumstances present in the manufacturing process by using a commercially available additive manufacturing machine and presented the experimental results for titanium alloy Ti-6Al-4V. Using this method, in the present study, we tried to measure the laser absorptivity for Inconel 718 and Inconel 738LC powders in addition to titanium alloy Ti-6Al-4V powder. We also modified the laser irradiation conditions to extend the measurement temperature range to higher temperatures than those used in the previous study.

2. Experimental Procedure

Laser absorptivity was measured using the calorimetric method employed previously, similar to the technique of Rubenchik *et al.* [4, 5]. The laser absorptivity was determined by analyzing energy conservation during the temperature alteration of a specimen irradiated by the laser.

To enable the use of a commercially available additive manufacturing machine, the laser irradiation conditions were chosen to ensure their feasibility for the machine's operation. The experimental setup was the same as that in the previous study, as shown in Fig. 1 [9]. The powder to measure laser absorptivity was spread out on a tray, and the

*Corresponding author, E-mail: HONDA.Hiroshi@nims.go.jp

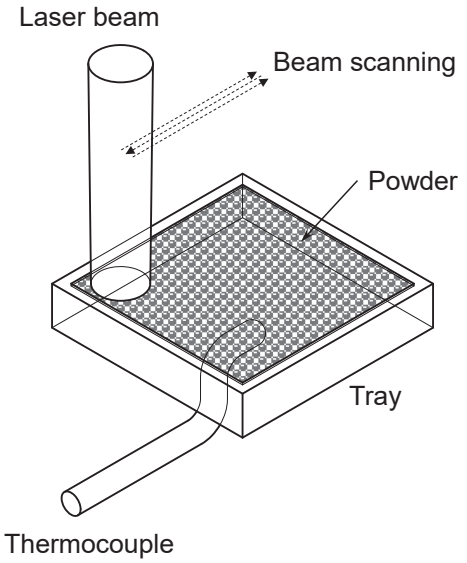

Fig. 1 Schematic of the experimental setup [9].

laser beam scanned the powder area repeatedly as shown in Fig. 1.

Laser absorptivity can be calculated by analyzing power conservation during the heating process induced by laser irradiation for a specimen consisting of a tray and powder. It can be written as follows:

$$A(T) = \frac{(m_1 c_1(T) + m_2 c_2(T))\Delta T + L(T)\Delta t}{E} \quad (1)$$

Here, t is time, T is temperature, and $A(T)$ is laser absorptivity at temperature T. m_1 and m_2 are the masses of the powder and tray, respectively. $c_1(T)$ and $c_2(T)$ are the specific heats of the powder and tray at temperature T, respectively. $L(T)$ is the thermal loss from the specimen to the surroundings at temperature T. E and ΔT are the irradiated energy and the temperature rise during the time interval Δt, respectively. The thermal loss can be evaluated from the specific heats and the cooling rate $\mathrm{d}T/\mathrm{d}t$ at temperature T as follows:

$$L(T) = -(m_1 c_1(T) + m_2 c_2(T))\frac{\mathrm{d}T}{\mathrm{d}t} \quad (2)$$

The thermal loss was estimated based on the temperature evolution during the cooling process following heating, with the cooling conditions maintained to be identical to those during heating in order to minimize the difference between the thermal losses during the heating and cooling processes.

The SLM Solutions SLM280 was used as a commercially available laser powder-bed fusion additive manufacturing machine. The laser was a Gaussian beam with a 1070 nm wavelength. The specimen was set in the machine's processing chamber. The chamber was filled with argon gas, mirroring the environment of the machine's manufacturing process.

The powders were commercially available. The Inconel 718 and Inconel 738LC powders used were Concept Laser CL 100NB and Höganäs Amperprint 0151, respectively. To compare the results with those of the previous study, laser absorptivity measurements were conducted for the titanium alloy Ti–6Al–4V powder as the laser irradiation conditions were changed from those in the previous study. The titanium alloy Ti–6Al–4V powder used was Concept Laser CL 41TI ELI. The tray material was titanium alloy Ti–6Al–4V, as in the previous study.

The tray dimensions were 10 mm × 10 mm × 1 mm, and its top surface had a machined recessed flat portion with a 0.10 mm depth. The flat recessed portion was filled flat with the metal powder up to the level of the rim. A thermocouple was attached to the center of the bottom surface of the tray to measure the temperature.

The mass of the tray was 0.4083 g. The powder masses were evaluated by measuring those on trays of the same shape. The masses of the nickel-base superalloy powders were in the ranges of 0.0273 ± 0.0018 g and 0.0332 ± 0.0006 g for Inconel 718 and Inconel 738LC, respectively. The mass of the titanium alloy Ti-6Al-4V powder was in the range of 0.0159 ± 0.0005 g. The errors of the masses represent the standard errors.

The laser beam was nearly perpendicular to the specimen and scanned the powder area in a meander hatch pattern as shown in Fig. 1. To prevent the metal powder from melting, the scan speed was set to high, which was estimated to be about 16 m/s. The spot size of the laser beam on the specimen was also expanded, which was estimated to be about 2.2 mm. The laser power was 50 W.

The laser was turned on while scanning along each hatch line and off while moving between lines. To reduce the non-irradiation time of the laser and increase the average power of laser irradiation on the specimen during the heating process, the time interval between scans of the meander hatch pattern was shortened compared to the previous study. The time interval in this experiment was estimated to be about 0.0339 s. The temperature around the laser irradiation point rises locally, with the increase becoming remarkable when the hatch lines are dense, due to rapid and repetitive heating. To increase the mean moving speed of the laser beam moving perpendicular to the hatch line and reduce the localized temperature rise around the laser irradiation point on the specimen, the number of hatch lines was also reduced compared to the previous study; in this experiment, there were 17 hatch lines in the powder area of the specimen. The scanning process of the meander hatch pattern was replicated 1000 times.

For the temperature-dependent specific heat used in the calculation of laser absorptivity, the fitting functions derived from experimental data were used. The fitting line for the titanium alloy Ti–6Al–4V [10] used in the calculation is drawn alongside the experimental data [11] in Fig. 2. The experimental data for Inconel 718 [12] and Inconel 738 [13] are also shown with the fitting lines used in the calculations.

3. Results and Discussion

Figure 3 illustrates the temperature history measured for the titanium alloy Ti-6Al-4V powder. Because the temperature sampling interval was 0.1 s, which was longer than the interval between scans of the meander hatch pattern, the temperature history's heating curve shows continuous heating without showing temperature changes corresponding to the time interval between scans of the meander hatch

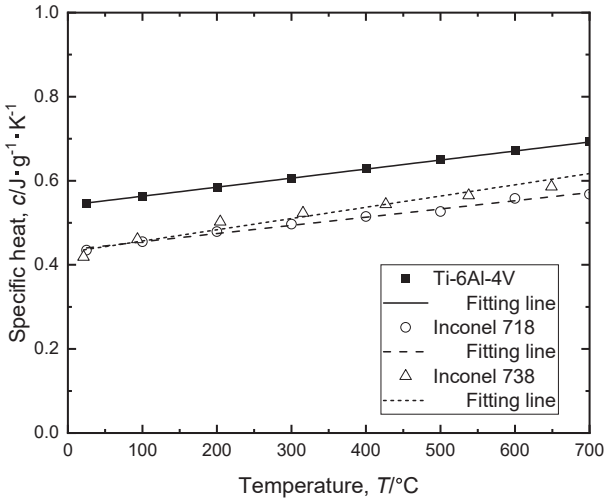

Fig. 2 Temperature dependencies of the specific heat of Ti-6Al-4V, Inconel 718, and Inconel 738 along with their respective fitting lines.

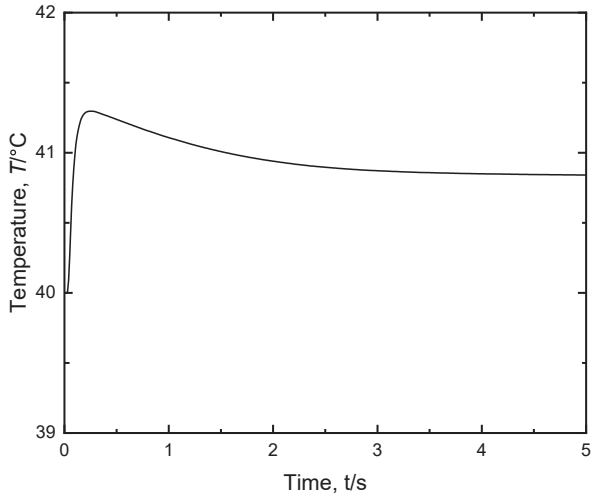

Fig. 4 Temperature variation at the center of the bottom surface in the numerical simulation with a single movement of the heat source.

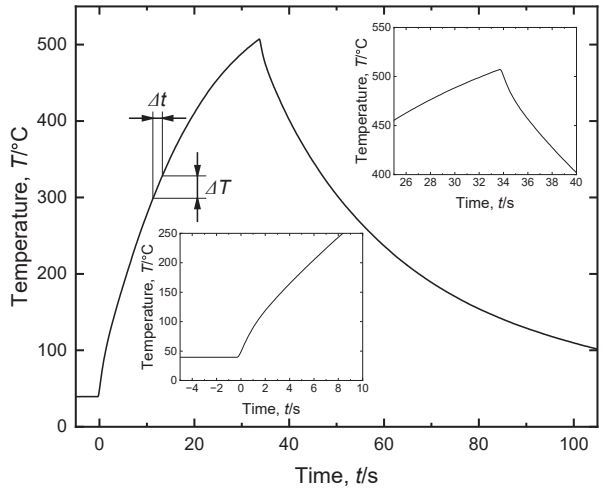

Fig. 3 Temperature history measured for the titanium alloy Ti-6Al-4V powder.

pattern. The values of ΔT and Δt for the laser absorption calculation in eq. (2) were determined as depicted in Fig. 3, and the value of Δt was set to 2 s.

As seen from the magnified temperature histories in the insets of Fig. 3, the cooling curve gradient changed notably around 35 s after the peak temperature was reached, while the heating curve gradient shifted around 2 s into the heating process. As considered in the previous study, these gradient changes are thought to be caused by the uniformization of the temperature distribution in the specimen.

To investigate the gradient changes, a simplified numerical simulation was performed as in the previous study. FEM calculations were conducted in the simulation using commercially available software, Wolfram Mathematica. A 2D model was adopted by assuming uniformity in the hatch line direction due to the laser beam's very high scan speed. Because the heat capacity of the powder is less than that of the tray, the calculation region was set as a rectangle 10 mm wide and 1 mm high, and consisted of a single material for simplification. The initial temperature within the calculation region was set at 40°C, with the boundary condition of the region indicating no thermal loss. A heat source placed on the top surface boundary of the region was moved from left to right corresponding to the movement of the laser beam in the perpendicular direction to the hatch line during scanning. The intensity profile of the heat source was adjusted to match the Gaussian shape corresponding to the laser irradiation intensity profile. The settings for the intensity profile included a laser power of 50 W and a spot diameter of 2.2 mm. The material of the calculation region for the simulation was titanium alloy Ti–6Al–4V. The physical property values of the material in the simulation were held as constants at 40°C. The laser absorptivity was assumed to be 0.6, which is the value measured for titanium alloy Ti–6Al–4V powder in the previous study.

Figure 4 shows the temperature history at the center of the bottom surface for the numerical simulation with a single movement of the heat source. The start time of the heat source movement was set to 0. The temperature rose as the heat distributed at the top surface propagated towards the center of the bottom surface, subsequently stabilizing to a constant value to homogenize the temperature distribution across the calculation region. The temperature became almost constant about 3 s after heating.

Considering the simulation result, the change in the cooling curve gradient around 35 s, seen in Fig. 3, is thought to be caused by the uniformization of the temperature distribution in the specimen. To eliminate this influence on the estimation of thermal loss from the cooling rate, the initial part of the cooling process from 3 s after the temperature was maximized was excluded from the estimation.

The measured temperature history after 3 s in the cooling process was smoothed and differentiated to estimate the cooling rate dT/dt in eq. (2). Figure 5 shows the estimated cooling rate plotted against temperature T for the cooling curve shown in Fig. 3. A fitting function of the plots is also shown. The thermal loss $L(T)$ was calculated from the fitting function of the cooling rate and the temperature-dependent specific heats of both the tray and the powder. This fitting function and the calculation of thermal loss were performed for each powder experiment.

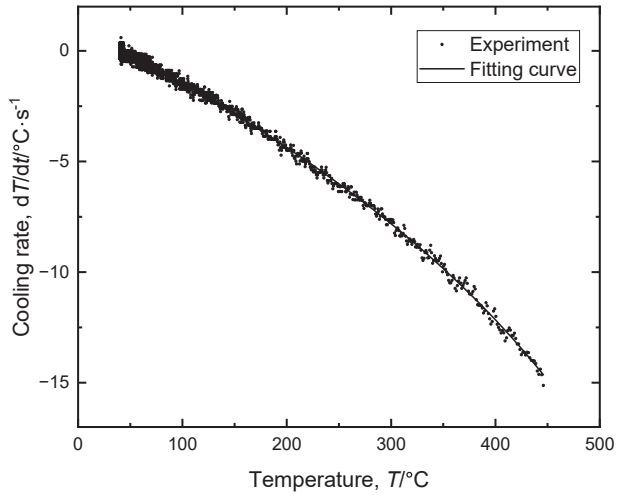

Fig. 5 Temperature dependence of cooling rate in the cooling process in Fig. 3 and its corresponding fitting curve.

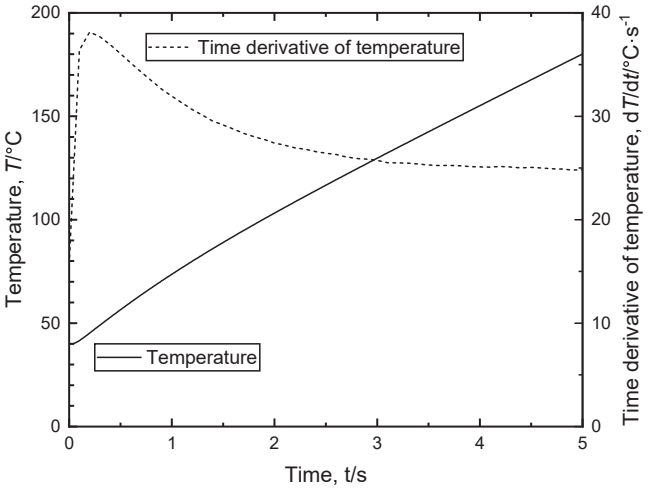

Fig. 6 Temperature variation and its time derivative at the center of the bottom surface in the numerical simulation with repeated movements of the heat source.

The temperature measured early in the heating process was also thought to be influenced by the uniformization of the temperature distribution. A 2D numerical simulation was performed to estimate the influence on the measured temperature history in the heating process. The simulation conditions were the same as those described above except for the repetition of the heat source movements at 0.0339 s intervals. The temperature history obtained from the simulation is shown in Fig. 6. The time derivative of the temperature is also shown in Fig. 6 to illustrate the temperature gradient more clearly.

Despite the lack of thermal loss, the temperature gradient undergoes a change for about 3 s, stabilizing to an almost constant level after this period. In the numerical simulation with a single movement of the heat source, it also takes about 3 s for the temperature to become almost constant. The change in the temperature gradient in the numerical simulation with multiple movements of the heat source is thought to be caused by the uniformization of the temperature distribution. The change in the heating curve gradient shown

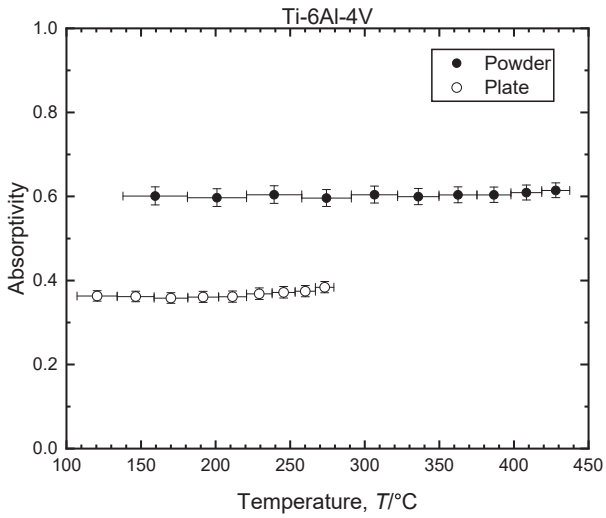

Fig. 7 Measured laser absorptivities of the Ti-6Al-4V powder and the Ti-6Al-4V tray.

in Fig. 3 is similar to that in the temperature gradient in the simulation and is attributed to the uniformization. Therefore, the initial segment of the heating process beginning 3 s after heating initiation was omitted from the laser absorptivity calculation to mitigate the impact of the temperature distribution homogenization process. Of course, the temperatures measured after 3 s are also influenced by the uniformization of temperature distribution. Nevertheless, the temperatures recorded from approximately 3 s after the start of heating include the influence of the uniformization at the same level. Consequently, it is plausible that the influence of the temperature difference ΔT on the calculation could be mitigated through cancellation.

Figure 7 shows the measured laser absorptivity data for the titanium alloy Ti–6Al–4V powder. The temperatures are intermediate values of upper and lower temperatures for ΔT calculation, and the range of error bars corresponds to the upper and lower temperatures. The temperatures employed for calculating laser absorptivity represent intermediary values between the upper and lower temperatures for ΔT calculation. The ranges of error bars of laser absorptivity are calculated from the upper and lower temperatures and the errors of the powder mass. In the previous study, the measurement temperature range of laser absorptivity was below 150°C. By changing the laser irradiation conditions, specifically the time interval of the scanning process in the meander hatch pattern, the temperature range was broadened, spanning from about 150°C to about 400°C. No significant temperature dependence of the laser absorptivity was seen in this temperature range. The laser absorptivity of the titanium alloy Ti–6Al–4V powder was about 0.6, which was almost the same as that for the same powder in the previous study.

The laser absorptivity of the tray without the powder was also measured. The laser absorptivity data for the machined flat surface of the titanium alloy Ti–6Al–4V tray are shown in Fig. 7. The laser absorptivity is labeled Plate. The laser absorptivity was about 0.37, which was almost the same as that for the tray in the previous study.

The laser absorptivity data measured for nickel-based superalloy Inconel 718 and Inconel 738LC powders are

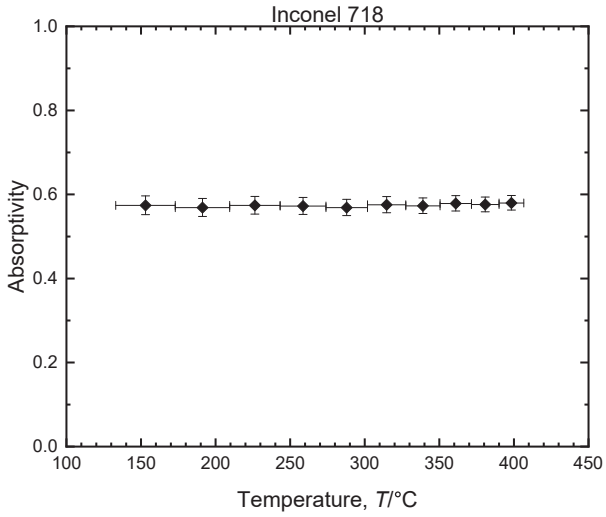

Fig. 8 Measured laser absorptivities of the Inconel 718 powder.

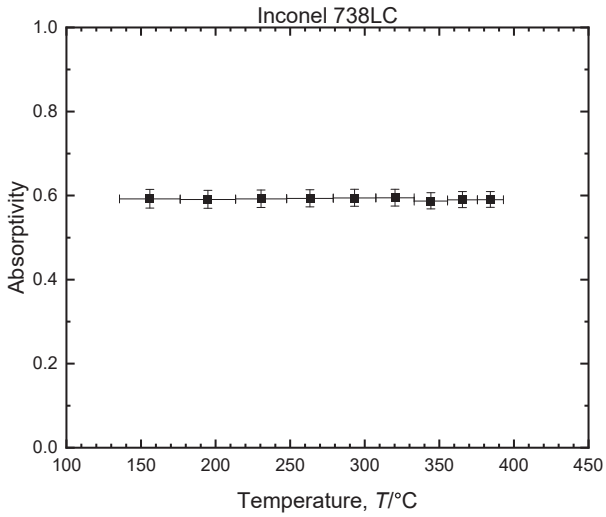

Fig. 9 Measured laser absorptivities of the Inconel 738LC powder.

shown in Figs. 8 and 9, respectively. The laser absorptivity values were calculated in the same manner as for the titanium alloy Ti–6Al–4V powder. The measurement temperature ranges were from about 150°C to about 400°C. No significant difference was observed in the laser absorptivities of Inconel 718 and Inconel 738LC powders, falling within the margins of error. The laser absorptivities were almost the same as those of the titanium alloy Ti–6Al–4V powder. The values were about 0.6, and no significant temperature dependencies were seen.

The values were slightly lower than the experimental value, about 0.67, of nickel-based superalloy Inconel 625 for the laser wavelength of 970 nm reported by Boley *et al.* [6], which was obtained by the calorimetric method [5]. In a study by Sainte-Catherine *et al.* [14], the laser absorptivity of the polished flat surface of Inconel 718 at a wavelength of 1.06 μm from an Nd-YAG laser was determined to be 0.30 at 300°C, utilizing an integrating sphere in atmospheric conditions. The ratio of the measured laser absorptivity of the powder to that of the flat surface was close to the value obtained from the ray-tracing simulation by Boley *et al.* [6].

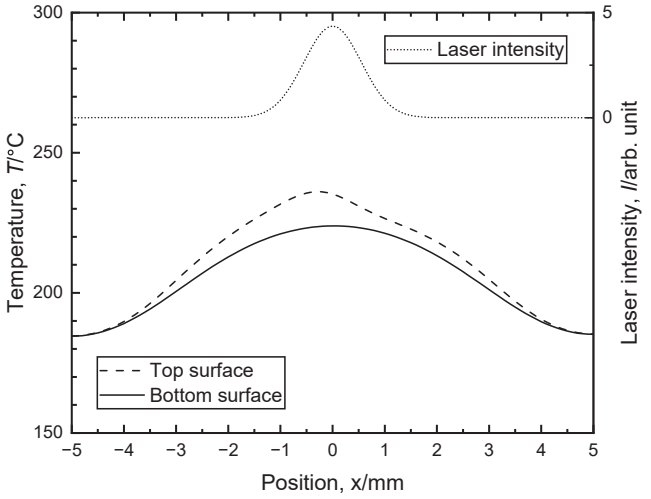

Fig. 10 Temperature distributions on the top and bottom surfaces and the laser intensity profile on the 200th movement of the laser from left to right in the numerical simulation.

Because the thermocouple couldn't be positioned at the laser irradiation point, the temperatures measured by the thermocouple attached to the center of the bottom surface are thought to differ from the actual temperature at the laser irradiation position. To check the difference in the temperatures, the temperature distribution was investigated by using the numerical simulation described above. The simulation conditions were the same as those for the simulation with multiple movements of the heat source. Figure 10 shows the temperature distributions on the top and bottom surfaces of the calculation region as well as the laser intensity profile on the 200th movement of the laser from left to right. The time was 6.76 s after the heat source started moving; this was later than the excluded time at the initial part of heating process described above.

The temperature distribution on the top surface exhibits significant convex nonuniformity across the entire specimen, showcasing a localized rise corresponding to the laser intensity profile. The local temperature rise was about 10 degrees Celsius, a decrease from a few tens of degrees Celsius in the previous study achieved by enhancing the mean moving speed of the laser beam perpendicular to the hatch line. However, the temperature on the top surface varies, ranging several tens of degrees Celsius due to the large convex nonuniformity. The nonuniformity seems to be caused by the overall laser intensity distribution on the specimen.

To examine the cause of the large convex nonuniformity, a numerical simulation similar to that described above, except for the laser irradiation conditions, was performed. In the simulation, the laser intensity distribution on the top surface comprised the time-averaged distribution encompassing all the intensity profiles of the hatch lines, with its position remaining fixed. The top surface was heated continuously by the fixed distribution. Figure 11 shows the simulation results of the temperature distributions on the top and bottom surfaces at 6.76 s after the commencement of heating, aligning with the time of the 200th movement in the simulation involving multiple movements of the heat source

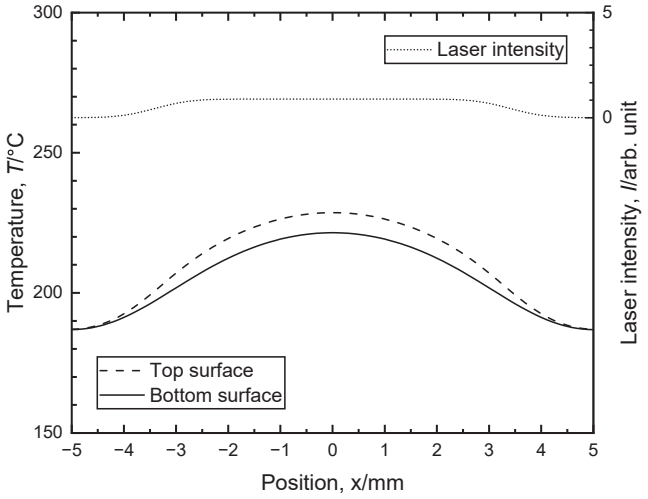

Fig. 11 Temperature distributions on the top and bottom surfaces and the laser intensity profile at 6.76 s in the numerical simulation of continuous heating.

as shown in Fig. 10. The laser intensity distribution, comprised of all the intensity profiles of the hatch lines, is also shown, appearing as a flat top with gradual slopes at the edges. The temperature distributions on the top and bottom surfaces show large convex nonuniformities, and the shapes of the distributions are almost the same as those shown in Fig. 10. Therefore, the large convex nonuniformity in temperature across the entire specimen is thought to stem from the laser intensity distribution generated by the meander hatch pattern with a broader Gaussian intensity profile and a smaller laser irradiation area than the specimen size.

The measured laser absorptivities in this experiment are presumed to be values averaged over such temperature variation ranges. Reducing the nonuniformity of the temperature distribution caused by the laser intensity distribution on the specimen is vital to achieve a more precise temperature-dependent laser absorptivity. In practical additive manufacturing operations, temperatures exceed the melting point. Therefore, it is necessary to extend the temperature range for laser absorptivity measurements to encompass higher temperatures.

4. Conclusion

We tried to measure the laser absorptivity of metal powders and their temperature dependence under identical conditions in laser powder-bed fusion additive manufacturing, employing a commercially available additive manufacturing machine.

We measured the laser absorptivities of nickel-based superalloy powders including Inconel 718 and Inconel 738LC, as well as titanium alloy Ti-6Al-4V powders. The measurement temperature ranges were about 150°C to about 400°C. The laser absorptivites of those powders were all about 0.6 at a laser wavelength 1070 nm. Within this range, no significant temperature dependence was observed for the laser absorptivity of these powders.

Acknowledgments

We would like to thank Mr. Masaru Suzuki for technical assistance with the experiments and Mr. Mitsugu Sato for preparation of the experimental devices.

REFERENCES

[1] B. Brandau, A. Da Silva, C. Wilsnack, F. Brueckner and A.F.H. Kaplan: Absorbance study of powder conditions for laser additive manufacturing, Mater. Des. **216** (2022) 110591.
[2] M. Haag, H. Hügel, C.E. Albright and S. Ramasamy: CO_2 laser light absorption characteristics of metal powders, J. Appl. Phys. **79** (1996) 3835–3841.
[3] T.J. Wieting and J.L. DeRosa: Effects of surface condition on the infrared absorptivity of 304 stainless steel, J. Appl. Phys. **50** (1979) 1071–1078.
[4] A.M. Rubenchik, S.S.Q. Wu, V.K. Kanz, M.M. LeBlanc, W.H. Lowdermilk, M.D. Rotter and J.R. Stanley: Temperature-dependent 780-nm laser absorption by engineering grade aluminum, titanium, and steel alloy surfaces, Opt. Eng. **53** (2014) 122506.
[5] A. Rubenchik, S. Wu, S. Mitchell, I. Golosker, M. LeBlanc and N. Peterson: Direct measurements of temperature-dependent laser absorptivity of metal powders, Appl. Opt. **54** (2015) 7230–7233.
[6] C.D. Boley, S.C. Mitchell, A.M. Rubenchik and S.S.Q. Wu: Metal powder absorptivity: modeling and experiment, Appl. Opt. **55** (2016) 6496–6500.
[7] J. Trapp, A.M. Rubenchik, G. Guss and M.J. Matthews: In situ absorptivity measurements of metallic powders during laser powder-bed fusion additive manufacturing, Appl. Mater. Today **9** (2017) 341–349.
[8] J. Ye, S.A. Khairallah, A.M. Rubenchik, M.F. Crumb, G. Guss, J. Belak and M.J. Matthews: Energy Coupling Mechanisms and Scaling Behavior Associated with Laser Powder Bed Fusion Additive Manufacturing, Adv. Eng. Mater. **21** (2019) 1900185.
[9] H. Honda and M. Watanabe: Quantifying Laser Absorptivity of Ti–6Al–4V Powder through Additive Manufacturing Systems, Mater. Trans. **65** (2024) 194–198.
[10] S. Sinha: Thermal model based simulation of nanosecond pulsed laser irradiation of Ti6Al4V alloy, J. Laser Appl. **31** (2019) 032008.
[11] K.C. Mills: *Recommended Values of Thermophysical Properties for Selected Commercial Alloys*, (Woodhead Publishing, 2002) pp. 211–217.
[12] K.C. Mills: *Recommended Values of Thermophysical Properties for Selected Commercial Alloys*, (Woodhead Publishing, 2002) pp. 181–190.
[13] *Alloy IN-738 Technical Data*, (The International Nickel Company, Inc.).
[14] C. Sainte-Catherine, M. Jeandin, D. Kechemair, J.P. Ricaud and L. Sabatier: STUDY OF DYNAMIC ABSORPTIVITY AT 10.6 µm (CO_2) AND 1.06 µm (Nd-YAG) WAVELENGTHS AS A FUNCTION OF TEMPERATURE, J. Phys. IV **01** (1991) C7-151–C7-157.